Biochimica et Biophysica Acta 1857 (2016) 1796–1806

Contents lists available at ScienceDirect

Biochimica et Biophysica Acta

journal homepage: www.elsevier.com/locate/bbabio

The cytochrome *b* Zn binding amino acid residue histidine 291 is essential for ubihydroquinone oxidation at the Q_o site of bacterial cytochrome bc_1

Francesco Francia [a], Marco Malferrari [a], Pascal Lanciano [b], Stefan Steimle [b], Fevzi Daldal [b,*], Giovanni Venturoli [a,c]

[a] Laboratorio di Biochimica e Biofisica Molecolare, Dipartimento di Farmacia e Biotecnologie, FaBiT, Università di Bologna, 40126 Bologna, Italy
[b] Department of Biology, University of Pennsylvania, Philadelphia, PA 19104, USA
[c] Consorzio Nazionale Interuniversitario per le Scienze Fisiche della Materia (CNISM), Dipartimento di Fisica, Università di Bologna, 40127 Bologna, Italy

ARTICLE INFO

Article history:
Received 11 February 2016
Received in revised form 27 June 2016
Accepted 17 August 2016
Available online 5 September 2016

Keywords:
Cytochrome bc_1 complex
Ubiquinol cytochrome *c* oxidoreductase
Bacterial photosynthesis and respiration
Q_o site inactivation and proton release
Zn binding

ABSTRACT

The ubiquinol:cytochrome (cyt) *c* oxidoreductase (or cyt bc_1) is an important membrane protein complex in photosynthetic and respiratory energy transduction. In bacteria such as *Rhodobacter capsulatus* it is constituted of three subunits: the iron-sulfur protein, cyt *b* and cyt c_1, which form two catalytic domains, the Q_o (hydroquinone (QH_2) oxidation) and Q_i (quinone (Q) reduction) sites. At the Q_o site, the pathways of bifurcated electron transfers emanating from QH_2 oxidation are known, but the associated proton release routes are not well defined. In energy transducing complexes, Zn^{2+} binding amino acid residues often correlate with proton uptake or release pathways. Earlier, using combined EXAFS and structural studies, we identified Zn coordinating residues of mitochondrial and bacterial cyt bc_1. In this work, using the genetically tractable bacterial cyt bc_1, we substituted each of the proposed Zn binding residues with non-protonatable side chains. Among these mutants, only the His291Leu substitution destroyed almost completely the Q_o site catalysis without perturbing significantly the redox properties of the cofactors or the assembly of the complex. In this mutant, which is unable to support photosynthetic growth, the bifurcated electron transfer reactions that result from QH_2 oxidation at the Q_o site, as well as the associated proton(s) release, were dramatically impaired. Based on these findings, on the putative role of His291 in liganding Zn, and on its solvent exposed and highly conserved position, we propose that His291 of cyt *b* is critical for proton release associated to QH_2 oxidation at the Q_o site of cyt bc_1.

1. Introduction

The ubihydroquinone:cytochrome (cyt) *c* oxidoreductase (cyt bc_1 or complex III of mitochondrial respiratory chain) catalyzes oxidation of hydroquinone molecules (QH_2) and reduces *c*-type cyts. The enzyme is an integral, homodimeric membrane complex formed of species-specific number of subunits (e.g., mitochondrial complex III contains up to 11 proteins). Three of these subunits, the Rieske iron-sulfur protein (ISP) with a high potential [Fe_2S_2] cluster, cyt c_1 with a *c*-type heme, and cyt *b* with one low and one high potential *b*-type (b_L an b_H, respectively) heme, always constitute the catalytic core of the enzyme [1]. These subunits also form two active domains, referred to as the QH_2 oxidation (Q_o) and quinone (Q) reduction (Q_i) sites, located at or near the *p* and *n* faces of energy transducing membranes, respectively. According to the Q-cycle mechanism [2], electrons resulting from QH_2 oxidation at the Q_o site are delivered to two different acceptor chains, while protons are released to the bulk water. The first electron is transferred to the high-potential electron acceptor chain, reducing sequentially the ISP Fe_2S_2 cluster and cyt c_1 heme. The second electron enters the low-potential chain located on cyt *b*, and is delivered to a Q (or a semiquinone, SQ) molecule at the Q_i site, via sequential reduction of the hemes b_L and b_H of cyt *b* [3]. Two turnovers of cyt bc_1 are required for the reduction of a Q molecule at the Q_i site, via the oxidation of two QH_2 at the Q_o site. This bifurcated electron transfer mechanism increases proton translocation efficiency of cyt bc_1, leading to the release of four protons per QH_2 oxidized, and uptake of two protons per Q reduced. Thus, the electron transfer reactions at the Q_o site couple the free energy difference between Q/QH_2 and electron acceptor *c*-type cyts to generate both a proton gradient and a membrane potential across the membrane, which are subsequently used for ATP biosynthesis.

Chromatophores (intracytoplasmic membrane vesicles) of non-sulfur purple bacteria, such as *Rhodobacter* (*R.*) *capsulatus*, which is

Abbreviations: cyt, cytochrome; DBH_2, decylbenzohydroquinone; E_h, ambient redox potential; E_m, midpoint redox potential; EXAFS, extended X-ray absorption fine structure; Fe_2S_2 cluster, iron-sulfur cluster; Q, ubiquinone; QH_2, ubihydroquinone; Q_o, hydroquinone oxidation site; Q_i, quinone reduction site; *R.*, *Rhodobacter*; RC, photochemical reaction center; SQ, seminquinone.

* Corresponding author.
E-mail address: fdaldal@sas.upenn.edu (F. Daldal).

http://dx.doi.org/10.1016/j.bbabio.2016.08.007
0005-2728/

readily amenable to genetic manipulations, contain a cyt bc_1 that is structurally similar and functionally analogous to that operating in mitochondria. In bacterial chromatophores, reducing and oxidizing substrates (QH_2 and ferricyt c_2, respectively) can be supplied to cyt bc_1 via the photosynthetic reaction center (RC). Following photoactivation, RC catalyzes vectorial electron transfer from the primary electron donor P (bacteriochlorophyll special pair) to the final electron acceptor Q bound at its Q_B site. The photo-oxidized P is re-reduced by ferrocyt c_2 on the periplasmic side, and upon a second photoactivation, a QH_2 is formed at the Q_B site with the uptake of two protons from the cytoplasmic side, and released to the membrane. The redox coupling between the RC and cyt bc_1 is mediated by the membrane Q/QH_2 pool and cyt c_2. Electron transfer steps of this cyclic pathway have been resolved by light activated kinetic spectrophotometry, performed under controlled ambient redox potential (E_h) (for reviews, see e.g. [4,5]).

Inhibitors of cyt bc_1 have been powerful tools in deciphering the electron transfer events of its catalytic cycle. These inhibitors are often Q analogs that bind competitively to the Q_o or Q_i sites, and their mechanisms of action have been characterized at both structural and functional levels [6–9]. Although several aspects of the catalytic mechanism of cyt bc_1 have been elucidated, structural identification of the pathways leading to proton uptake and release by cyt bc_1 is still unclear. Aside the Q analogs, another group of cyt bc_1 inhibitors are divalent metal ions such as Zn^{2+} and Cd^{2+} [10,11]. These ions are inhibitory not only for cyt bc_1 but also for other proton translocating membrane enzymes, such as the NADH:ubiquinone oxidoreductase [12,13], transhydrogenase [14,15], cyt *c* oxidase [16] and the bacterial RC [17], for which the inhibitory mechanism of Zn^{2+} and Cd^{2+} has been well characterized. The metal binding site is located at the cytoplasmic surface and is formed of His and Asp residues, involved in the proton transfer reactions required for reduction of Q at the Q_B site of the RC [18,19]. Accordingly, binding of the metal ion obstructs the proton entry point, directly competing with binding of protons to the His residues. Studies on other proton translocating membrane complexes showed that at least one His residue is always present among the metal binding ligands, suggesting a common mechanism for metal ion mediated inhibition [20–22].

The X-ray structure of the mitochondrial cyt bc_1-Zn^{2+} complex, obtained by soaking pre-formed crystals of avian complex with Zn^{2+} revealed two metal binding sites [23]. One of them has high binding affinity, is located in a hydrophilic area between the cyt *b* and cyt c_1 subunits in the vicinity of the Q_o site, suggesting that it interferes with proton egress from this site. Extended X-ray absorption fine-structure (EXAFS) spectroscopy studies of non-crystallized cyt bc_1-Zn^{2+} complexes provided results consistent with the crystal structure of the avian mitochondrial cyt bc_1-Zn^{2+} complex, and allowed identification of the residues forming a tetrahedral binding cluster [20]. The EXAFS studies were also extended to the bacterial enzyme, and showed that the Zn^{2+} binding site of cyt bc_1 purified from the photosynthetic bacterium *R. capsulatus* is structurally superimposable with those of the avian and bovine complexes, but had a different pseudo-octahedral coordination. On the basis of EXAFS and superimposition of the 3D structures of bacterial cyt bc_1 with that of Zn^{2+} containing avian counterpart, we proposed that the bacterial binding cluster is formed of His276, Asp278, Asn279, and Glu295 residues of cyt *b* (*R. capsulatus* numbering) and two water molecules (Fig. 1) [20]. Moreover, we showed that the EXAFS data were also compatible with an alternative cluster, which in addition to His276 and Asp278, involved a second His residue (His291) and three water molecules possibly participating in a pseudo-octahedral coordination [20]. Interestingly, these residues are located in a highly hydrophilic portion of the Q_o site, with His291 residue facing directly the water phase, thereby suggesting an exit pathway for protons released by QH_2 oxidation [26].

In order to experimentally probe the catalytic role (if any) of the cyt *b* His276, Asp278, Asn279, Glu295 and His291 residues highlighted by

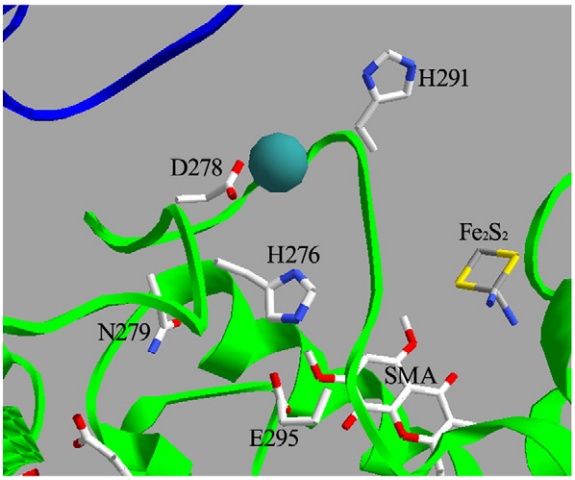

Fig. 1. Putative amino acid residues involved in binding Zn^{2+} to bacterial cyt bc_1. The side chains of Glu295, Asn279, His276 and Asp278 of cyt *b* of *R. capsulatus* cyt bc_1, which are proposed to be the potential Zn^{2+} ion ligands, are colored in CPK. The critical His291residue, which might also be involved in Zn^{2+} binding, is shown together with the iron sulfur (Fe_2S_2) center of the ISP subunit and stigmatellin (SMA) bound to the Q_o site. The cyt *b* and cyt *c* subunits are depicted in green and blue, respectively, but the ISP subunit is omitted for visual clarity. One of the propionate groups of cyt b_L heme is visible in the lower left corner. Zn^{2+} ion (blue sphere) was superimposed after alignment of the *R. capsulatus* bc_1 structure (PDB entry 1ZRT [24]) with that of the Zn crystal of the chicken complex (PDB entry 3H1K [23]). As indicated by sequence alignments, *R. capsulatus* cyt *b* residues E295, H291, N279, D278, H276 correspond to residues E271, H267, N255, D254, D252 respectively in the *B. taurus* sequence, and to residues E272, S268, N256, D255, H253 in the *S. cerevisiae* sequence [25].

the EXAFS studies, we substituted each of them with a non-proton accepting side chain. Among these residues, Glu295Val mutation had already been studied earlier [27–29]. Using Zn^{2+} inhibition kinetics, isothermal titration calorimetry and Fourier transformed IR spectroscopy we had shown that this residue bound Zn^{2+} which decreased cyt bc_1 activity, suggesting that it could be involved in proton efflux coupled to electron transfer at the Q_o site. However, its function has been found to be not essential, inferring that in its absence some other residues could still carry out partly its role in QH_2 oxidation [27].

In the present work, we determined the effects of similar mutations at the remaining putative Zn^{2+} ligands, and showed for the first time that the cyt *b* His291Leu mutant was completely unable to support photosynthetic growth of *R. capsulatus*. By characterizing the properties of His291Leu mutant, including the spectral and redox properties of its cyt b_L and b_H hemes, as well as its light-activated cyt *b* reduction and cyt *c* re-reduction kinetics, we established that this mutation dramatically inhibited electron transfer from QH_2 oxidation to both the high and low potentials chains, yielding an assembled but almost inactive enzyme. Importantly, we showed that the kinetics of proton ejection associated with QH_2 oxidation at the Q_o site was also drastically inhibited in the His291Leu mutant. Based on overall data, the location and the highly conserved nature of H291, we concluded that this residue is essential for cyt bc_1 Q_o site catalysis, and suggest that it may be critical for proton-coupled electron transfer reactions during QH_2 oxidation.

2. Materials and methods

2.1. Bacterial strains, growth conditions, and genetic crosses

Escherichia coli strains harboring the pMTS1-derivative plasmids [30] with cyt *b* mutations were in HB101 background (F^- Δ(*gpt-proA*)*62 araC14 leuB6*(Am) *glnV44*(AS) *galK2*(Oc) *lacY1* Δ(*mcrC-mrr*) *rpsL20*(Str^r) *xylA5 mtl-1 thi-1*). They were grown at 37 °C in LB medium supplemented with 12.5 μg/ml tetracycline (Tet), as appropriate. The

pMTS1-derivative plasmids expressing the cyt bc_1 mutants were introduced into the *R. capsulatus* strain MT-RBC1 [Δ(*petABC::spe*)], which has a complete chromosomal deletion of *petABC* [31] using triparental mating, as described earlier [32]. These mutants were grown at 35 °C (except His291Leu which grew better at 28–30 °C) under respiratory (Res, aerobic dark) or photosynthetic (Ps, anaerobic light) conditions in liquid (one liter culture in two liters flasks) or solid (Petri dishes) MPYE enriched medium, supplemented with 10 μg/ml kanamycin (Kan), as described earlier [33]. Plates were incubated in temperature-controlled incubators (Percival, Inc.) in the dark (Res) or in anaerobic jars with $H_2 + CO_2$ generating gas packs (Becton Dickinson Inc., MD) in the light (Ps).

2.2. Molecular genetic techniques

Molecular genetic techniques were performed using standard procedures [34], as described earlier [35]. All constructs were verified by DNA sequencing, and analyzed using MacVector (Accelerys, San Diego, CA). Cyt *b* mutations were obtained via the "QuickChange™ Site-Directed Mutagenesis kit" (Stratagene Inc., La Jolla, CA), using the plasmid pPET1 carrying the wild type *petABC* operon [31] as a template, and the pairs of forward (F) and reverse (R) mutagenic primers H276L-F: 5′-CGA ACT ACC TCG GCC TCC CGG ACA AC and H276L-R: 5′-GTA GTT GTC CGG GAG GCC GAG GTA G; D278V-F: 5′-CTC GGG CAC CCG GTC AAC TAC GTC CA and D278V-R: 5′-CTG GAC GTA GTT GAC CGG GTG GCC G; N279L-F: 5′-GGC CAC CCG GAC CTC TAC GTC CAG GC and N279L-R: 5′-GGC CTG GAC GTA GAG GTC CGG GTG G; H291L-F: 5′-CTC GAC CCC GGC GCT TAT CGT TCC GG and H291L-R: 5′-CAT TCC GGA ACG ATA AGC GCC GGG G to yield the plasmids pPET1-B:H276L, pET1-B:D278V, pPET1-B:N279L and pPET1-B:H291L, respectively. The *Xma*I-*Stu*I fragment of pMTS1 was then exchanged with its counterparts from appropriate pPET1 derivatives with the desired mutations to yield the plasmids pMTS1-B:H276L, pMTS1-B:D278V, pMTS1-B:N279L and pMTS1-B:H291L, respectively.

2.3. Biochemical techniques

Chromatophore membranes were prepared as described in [36] and routinely resuspended in small volumes of 50 mM MOPS, pH 7.00, kept at 4 °C, and used within a maximum of six days. At variance, for measurements of proton release, as probed by the pH-indicator Neutral red (see Section 3.5), cells were washed in 10 mM MOPS, pH 7.5, and the chromatophores pellet was washed twice in a 2 mg/ml bovine serum albumin solution at pH 7.5. The bacteriochlorophyll content was estimated upon extraction with methanol/acetone (7:2), as described in [37]. Protein concentrations were determined using the bicinchoninic acid with bovine serum albumin as a standard [38] and SDS-PAGE (12.5%) was conducted as described in [39]. Prior to loading, samples were solubilized in a loading buffer at a final concentration of 62.5 mM Tris-HCl pH 6.8, 2% SDS, 0.1 M dithiothreitol, 25% glycerol, and 0.01% bromophenol blue by incubation at room temperature for 10 min. Immunoblot analyses were carried out as in [40] using rabbit polyclonal antibodies specific for *R. capsulatus* cyt bc_1 subunits. Alkaline phosphatase conjugated *anti*-rabbit IgG antibodies (Sigma Inc.) were used as secondary antibodies, and signal detection was via the BCIP/NBT-purple liquid substrate (Sigma, Inc.).

Steady-state cyt bc_1 activity was measured using decylbenzohydroquinone (DBH_2) as an electron donor and horse heart cyt *c* as an electron acceptor at 25 °C [41]. The reaction was initiated by addition of chromatophore membranes, monitored at 550 nm for 1 min, and the portion of the initial rate that is sensitive to famoxadone (a Q_o site inhibitor) was taken as the enzyme activity. Optical spectra were recorded on a Cary 60 spectrophotometer (Agilent Technologies Inc.).

2.4. Spectroscopic techniques and data analysis

For dark equilibrium redox titrations, chromatophore membranes were resuspended in 50 mM MOPS, 100 mM KCl, pH 7.00 in the presence of 50 μM 2,3,5,6-tetramethyl-*p*-phenylenediamine (DAD), 40 μM duroquinone, and 20 μM each of phenazine ethosulfate, phenazine methosulfate, 1,2-naphthoquinone, 1,4-naphthoquinone, and 2-hydroxy-1,4-naphthoquinone used as redox mediators. Optical spectra of chromatophore membranes, between 530 and 590 nm, were acquired with a Jasco V-550 spectrophotometer, as a function of the ambient redox poise (E_h) of the sample kept anaerobic under a stream of argon. The ambient redox potential E_h, measured by a platinum electrode against an external calomel electrode, was changed by addition of a concentrated solution of potassium ferricyanide as an oxidant, and sodium ascorbate or sodium dithionite as reductants. The values of the midpoint potential (E_m) of the cyt *b* hemes were determined by fitting the absorbance $A(E_h)$ (recorded at 560–540 nm as a function of E_h) to the sum of three Nernstian components ($i = 3$), according to:

$$A(E_h) = \sum_{i=1}^{3} A_i \left\{ 1 + exp\left[(E_h - E_{mi}) \frac{nF}{RT} \right] \right\}^{-1} \quad (1)$$

where for each component i, A_i and E_{mi} are the absorbance of the totally reduced form and the midpoint potential, respectively, and $n = 1$ is the number of electrons. *T* refers to the absolute temperature, and *R* and *F* to the gas and Faraday constants. Confidence intervals within two standard deviations (σ) in the determination of the contribution (A_i) and midpoint potentials (E_{mi}) of the different cyt *b* hemes were evaluated numerically as described earlier [42].

For kinetic spectrophotometry of flash-induced cyt *c* and cyt *b* redox changes, as well as of carotenoid electrochromic signals, chromatophore membranes were resuspended in 50 mM MOPS, 100 mM KCl, pH 7.00, at controlled E_h conditions under an atmosphere of nitrogen. The redox mediators 1,2-naphthoquinone, 1,4-naphthoquinone and *p*-benzoquinone at 8 μM, and phenazine methosulfate and phenazine ethosulfate were used at 1 μM. When appropriate, 10 μM valinomycin, 5 μM antimycin, 2 μM myxothiazol and 1 μM stigmatellin were added to the samples.

In proton release measurements, absorption transients of Neutral red after a single flash were measured at 546 nm in chromatophore suspensions buffered (pH = 7.5) by the membrane impermeable bovine serum albumin (2 mg/ml) in the presence of 1 mM Na-Ascorbate, 10 μM DAD, 1 mM KCN, 1 μM oligomycin, 50 mM KCl, 5 μM valinomycin.

The electron transfer chain was activated by a Xenon flash lamp (EG&G, Inc., FX201), discharging a 3 μF capacitor previously charged to 1.5 kV. The flash light (duration ~4 μs at half maximal intensity) was filtered through two layers of Wratten 88A gelatin filters (Kodak, Inc.). Absorbance changes were measured using a single-beam spectrophotometer of local design as described in [43]. Flash-induced electrochromic carotenoid band shift kinetics was measured at 503 nm [44], the kinetics of total cyt *c* (cyt c_1 + cyt c_2 + cyt c_y) redox changes were monitored at 550–540 nm [45], and those of cyt *b* were recorded at 560–543 nm. Spectra of flash-induced absorption changes, measured both in wild-type and mutant chromatophores (not shown) indicated that this wavelength couple minimized optical interference due to other redox components of the electron transfer chains in chromatophore membranes. The concentration of the primary electron donor P of the RC photoxidized by a single flash was estimated from the absorbance changes induced at 542 nm using an extinction coefficient $\varepsilon_{542} = 10.3\ mM^{-1}\ cm^{-1}$ [46]. To avoid fast, unresolved re-reduction of P^+ by cyt c_2 following a flash of light, measurements were performed at an ambient redox potential of $E_h = 420$ mV, at which the main endogenous electron donor to P^+, cyt c_2 ($E_m = 350$ mV [47]), is completely pre-oxidized in the dark. For the P^+/P couple, a E_m value of 440 mV was assumed [48] for correcting

the fraction of the primary donor pre-oxidized at the redox poise of the measurement.

Figs. 1 and 7 were generated using the Swiss-PdbViewer software (http://www.expasy.org/spdbv/) [49].

3. Results and discussion

3.1. Mutations of the Zn^{2+} binding ligands of cyt bc_1

The possible Zn^{2+} liganding residues located in *R. capsulatus* cyt *b* have been identified earlier (Fig. 1) [20]. Of these residues the Glu295 was studied by various groups [27–29], and its implications into the proton release from the Q_o site was probed [50]. In this work, using *R. capsulatus* we substituted the remaining Zn^{2+} liganding residues (His276, Asp278, Asn279, and His291) with no proton donor/acceptor side chains (e.g., Leu or Val) in order to assess their role(s) in QH_2 oxidation at the Q_o site (Fig. 1). Initial characterizations of these cyt *b* mutants, including their ability to support Ps growth of *R. capsulatus* (which requires an active cyt bc_1), SDS-PAGE/immunodetection with subunit-specific antibodies and the steady-state DBH_2: cyt *c* reductase activity indicated that only the His291Leu substitution yielded a cyt bc_1 variant that was assembled but unable to support Ps growth and that exhibited extremely low enzymatic activity (< 5% of wild type) (see Supplementary material, Fig. S1A and B). These findings led us to examine in detail the salient properties of the cyt *b* H291Leu mutant, which are described below. The remaining cyt *b* His276Leu, Asp278Val and Asn279Leu mutants that yielded partly active cyt bc_1 variants will be discussed elsewhere.

3.2. Spectral and redox properties of the cyt b hemes in wild type and His291Leu mutant

The redox difference absorption spectra recorded between 530 nm and 585 nm during reductive titrations of chromatophore membranes from wild type (WT) and His291Leu mutant (H291L), at comparable bacteriochlorophyll (Bchl) concentrations, are shown in Fig. 2A and B, respectively. The spectra recorded at the highest value of ambient redox potential (E_h = 371 mV for WT, E_h = 331 mV for H291L mutant) were subtracted from each spectrum measured at lower E_h values, between ~230 mV and ~−190 mV, and the difference spectra offset to zero absorbance at 540 nm for visual clarity. In the wild type (WT) spectra, upon lowering E_h below ~230 mV, spectral contribution of the *c*-type cyts that peak at 550 nm increased slightly, and a second band (centered at 560 nm) appeared progressively, corresponding to the reduced cyt *b* hemes [51]. Upon decreasing E_h, the His291Leu mutant also exhibited an increasing spectral contribution centered at 560 nm, consistent with the progressive reduction of *b*-type cyts. The maximal absorbance change detected at 560 nm was about three times lower in the mutant, as compared to WT chromatophores, suggesting a lower content of cyt bc_1. Note that in the His291Leu mutant, the smaller amplitude of the cyt *c* peak at 550 nm relative to that at 560 nm, was due to the lower redox potential (E_h of 331 mV) of the spectrum used as a baseline, as compared to that (E_h of 371 mV) subtracted from the wild type spectra. Assuming a differential extinction coefficient of 20 mM^{-1} cm^{-1} for the 560–570 nm wavelength couple [41], a total *b*-heme concentration ~3.4 μM and ~0.9 μM was estimated using the spectra recorded at the lowest E_h values for the wild type and the His 291Leu, corresponding to cyt *b*/BChl ratios of ~0.045 and ~0.014, respectively.

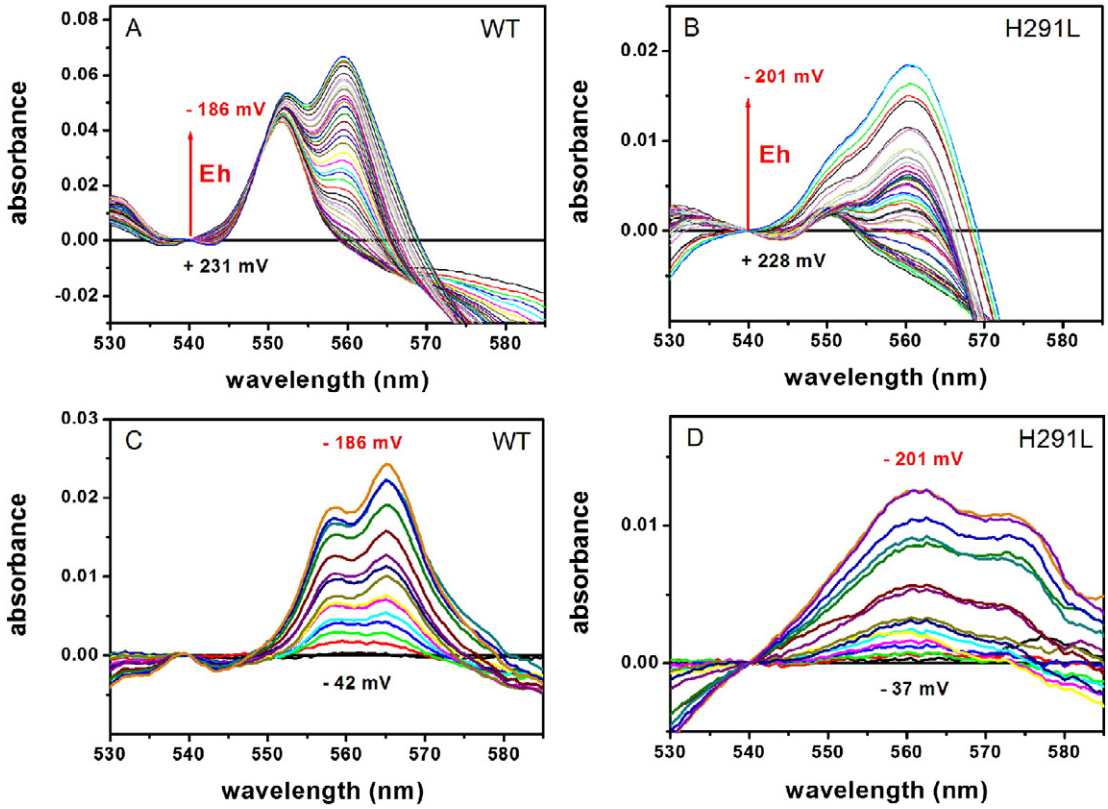

Fig. 2. Full spectrum dark redox titrations of cyt *b* hemes in wild type and cyt *b* His291Leu mutant strains. Spectra were obtained using wild type (WT, panel A) and His291Leu (H291L, panel B) chromatophore membranes suspended at 76 and 63 μM Bchl, respectively. The spectra were offset to zero at 540 nm for visual clarity, and red arrows indicate the direction of the reductive titrations. The E_h values reported in black and red in each panel refer to the difference spectra obtained under the most oxidizing and reducing conditions respectively, considered when analyzing the redox titrations (see Fig.3). Spectral contributions of heme b_L were extracted from the titration data, and presented in panels C (WT) and D (H291L). See Section 3.2 for further details.

Spectra of the low potential heme b_L were extracted from the titration data set by subtracting the spectrum recorded at an E_h value of −27 mV from each of the spectra recorded at lower E_h values. The E_m values reported in the literature [27] for heme b_H ($E_m = 45$ mV) and for heme b_L ($E_m = -130$ mV) indicated that at this E_h value the latter should be totally oxidized, and the former already pre-reduced. As expected, the spectra obtained by this procedure using wild type chromatophores (Fig. 2C, WT) exhibited the typical features of heme b_L, i.e. a peak at 566 nm and a lower one around 558 nm [46]. In contrast, the spectra obtained using mutant chromatophores showed a major peak between 562 and 564 nm and a second one of lower amplitude, at ~574 nm (Fig. 2D, H291L). Additionally, in the case of the mutant spectra, the absorption bands were much broader than those seen with the wild type spectra. The spectral broadening due to the His291Leu mutation suggested that the cyt *b* hemes environments in the mutant cyt bc_1 were perturbed [52]. This implied that the local structural perturbation induced by the His291Leu mutation propagates through long-range intramolecular interactions from the surface of the complex (see below) to the cyt *b* heme transmembrane region. The possibility that a single-site mutation can reverberate through the protein structure over long distances (up to 20 Å) resulting in dynamic and structural changes to distal sites is well documented in the literature (see, e.g., [53–57]).

Next, the dependence of the absorbance changes at 560–540 nm upon the redox potential (E_h) was fitted to the sum of three one-electron Nernst components, as described above in Eq. (1) (Materials and methods) in order to compare the E_m values of the cyt *b* hemes in the wild type (WT) and His291Leu mutant chromatophore membranes (Fig. 3). The values obtained by the "best fit" procedure for the relative amplitudes A_i and E_{mi} of the different components are summarized in Table 1. The highest E_m component ($E_{m1} = 105$ mV and $E_{m1} = 123$ mV for wild type and His291Leu, respectively) was attributed to the so-called cyt b_{150} component of cyt bc_1 [58]. The cyt b_{150} was suggested to arise from the mechanism of reduction of Q at the Q_i site of cyt bc_1. Namely, the equilibrium constant for cyt b_{150} formation is known to depend on the association (binding) constants of QH_2 and Q, and the equilibrium between heme b_H and the semiquinone SQ/QH_2 couple at the Q_i site of cyt bc_1 [59]. No major difference was seen between the wild type and the His291Leu mutant chromatophores in respect to this component (Fig. 3A and B). Similarly, the second redox component, ascribed to heme b_H [27,58] is present in both wild type and His291Leu titrations, with E_{m2} values of about 36 mV and 40 mV, respectively. The third spectral component, characterized by the lowest midpoint potential, was attributed to heme b_L [27,58], and showed E_{m3} values of −133 mV and −141 mV in the case of the wild type and mutant His291Leu, respectively. The amplitude of the third Nernstian component is larger in the mutant, as compared to wt (Table 1). This is related to the broadening and distortion of the corresponding spectrum in the mutant (see Fig. 2 C and D). Since the extinction coefficients for heme b_H and b_L individually at the wavelength couple used are not known in the mutant, the amplitude of the respective Nernstian components cannot be taken as reflecting the effective stoichiometries of the *b* hemes within the complex.

Overall, analyses of dark redox equilibrium titrations data indicated that the E_m values obtained using wild type chromatophores for the hemes b_H and b_L of cyt bc_1 were in good agreement with earlier reported values [27]. Moreover, within the calculated confidence intervals, the mutant His291Leu exhibited E_m values not significantly different from those of wild type for both these cofactors of cyt bc_1 (Table 1). We therefore concluded that although the His291Leu mutation affected the environments of cyt b_L and b_H hemes, it did not modify significantly their E_m values.

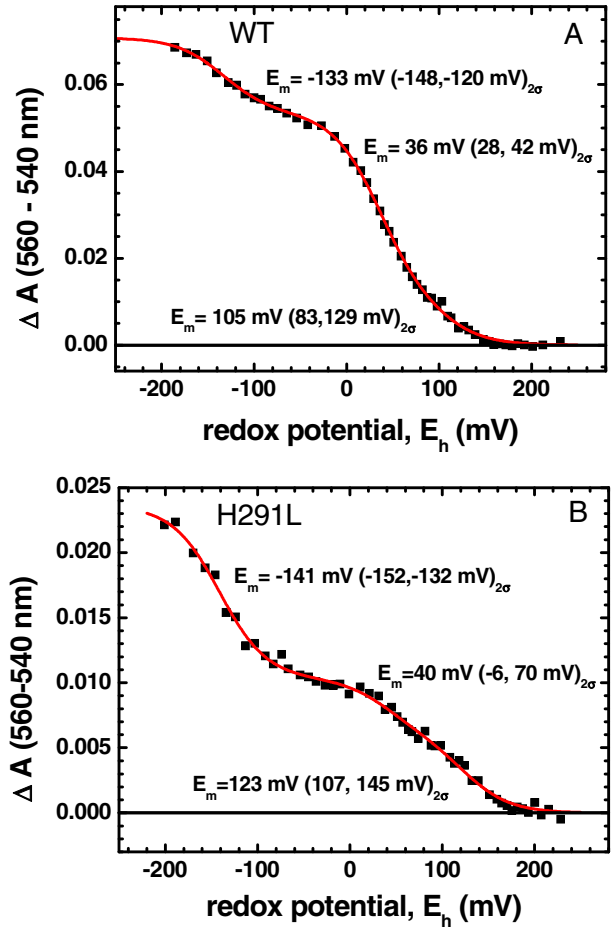

Fig. 3. Equilibrium redox titrations of cyt *b* hemes in wild type and cyt *b* His291Leu mutant strains. The titration data derived from the spectra shown in Fig. 2 were used. Absorbance changes at 560–540 nm, plotted as a function of the ambient redox potential (E_h), were fitted to the sum of three, one-electron, Nernstian components, according to Eq. (1) (see the text). Best fitting curves are shown as continuous red lines. The corresponding E_m values are indicated, with 2σ confidence intervals shown in brackets. The relative contributions of the three different cyt *b* components are summarized in Table 1.

3.3. Effects of His291Leu mutation on flash-induced electrochromic carotenoid signals

The membrane potential resulting from electrogenic events that occur during the photo-activated cyclic electron transfer chain in chromatophores can be followed by monitoring the electrochromic response of carotenoids embedded in the light harvesting complex (LH) II [60]. Upon activation of dark-adapted, freshly prepared chromatophore membranes of a wild type strain (WT) by a single turnover flash under E_h controlled and reducing conditions, a carotenoid electrochromic signal formed of three kinetic phases can be detected (Fig. 4A, black trace) [4,60]. The first two phases (I and II), completed within a few microseconds (not kinetically resolved in the traces shown in Fig. 4A) reflect the electrogenic events within, and the electrogenic oxidation of cyt c_2 + cyt c_y by the photo-oxidized primary electron donor P of, the RC. Accordingly, phase (I + II) is totally unaffected by electron transfer inhibitors of cyt bc_1 (Fig. 4A, blue trace). In the ms time scale, a third slower phase (phase III), which is due to the electrogenic events occurring in cyt bc_1, can also be detected [60,61]. Using the Q_i site inhibitor antimycin, which blocks electron transfer from heme b_H to Q bound at this site, phase III can be further resolved into antimycin-sensitive and antimycin-insensitive phases [62].

Table 1
Relative contribution (A_i) and midpoint potential (E_{mi}) obtained for each redox component by fitting the equilibrium dark redox titrations of cyt *b* hemes shown in Fig. 3 to Eq. (1). Values indicated between the parentheses refer to the extremes of the confidence intervals within 2 standard deviations (2σ). WT and H291L correspond to the wild type and the cyt *b* His291Leu mutant strains, respectively.

	A_1 (%)	E_{m1} (mV)	A_2 (%)	E_{m2} (mV)	A_3 (%)	E_{m3} (mV)
WT	13	105	63	36	24	−133
	(7, 24) $_{2\sigma}$	(83, 129) $_{2\sigma}$	(51, 68) $_{2\sigma}$	(28, 42) $_{2\sigma}$	(21, 28) $_{2\sigma}$	(−148, −120) $_{2\sigma}$
H291L	26	123	18	40	56	−141
	(14, 35) $_{2\sigma}$	(107, 145) $_{2\sigma}$	(9, 28) $_{2\sigma}$	(−6, 70) $_{2\sigma}$	(50, 61) $_{2\sigma}$	(−152, −132) $_{2\sigma}$

Addition of the Q_o site inhibitor myxothiazol, which blocks electron transfer to heme b_L, totally eliminates phase III (Fig. 4A, red trace).

In contrast to the wild type (WT), in chromatophores from the His291Leu mutant, the amplitude of phase III, relative to phase (I + II), was highly reduced (Fig. 4B, black trace). Moreover, the onset kinetics of phase III were severely slowed down in the His291Leu mutant, with the half time of the myxothiazol sensitive phase III (~2.5 ms in WT) increasing to values larger than 13 ms. Indeed, the two components of phase III (Figs. 4C and D) were both retarded in the mutant: the half-time of the antimycin-sensitive phase (blue trace), that is ~2.7 ms in WT, was larger than 13 ms in H291L chromatophores, and the half-time of the antimycin-insensitive (myxothiazol sensitive) phase (red trace), ~1.8 ms in WT, increased to values larger than 11 ms in the mutant. The data clearly indicated that the rates of the electrogenic events occurring in cyt bc_1 following a single turnover photo-excitation of the RC were markedly inhibited in the His291Leu mutant, even though the E_m values of the cofactors were unchanged.

3.4. Effects of His291Leu mutation on cyt c and cyt b reduction single turnover kinetics

The kinetics of cyt *c* and cyt *b* redox changes following flash photo-activation of RC under reducing conditions, and their responses to inhibitors of cyt bc_1 provide insights into the decreased enzyme turnover, as seen by the lower steady-state cyt bc_1 enzymatic activity (see Supplementary material, Fig. S1A), and the slower kinetics of phase III of the carotenoid signal in the His291Leu mutant (Fig. 4). In chromatophores that are redox poised at an E_h value of about 110 mV, the high potential chain cofactors of cyt bc_1 (ISP Fe_2S_2 cluster, cyt c_1 and cyt c_2) are pre-reduced in the dark, while the low potential chain cofactors (hemes b_L and b_H) are pre-oxidized. Following photo-activation by an actinic flash, the photo-oxidized primary electron donor P^+ of RC rapidly oxidizes ferrocyt c_2, which receives an electron derived from the high potential chain of cyt bc_1, namely from cyt c_1 that in turns receives it from the ISP Fe_2S_2 cluster. The Fe_2S_2 cluster thus oxidized then oxidizes QH_2 [63], receiving its first electron to form a transient SQ at the Q_o site. The large-scale movement of the extrinsic domain of the ISP conveys this electron from the Q_o site at the surface of cyt *b* to near cyt c_1 to reduce it [7,64]. The total cyts *c* (c_1, c_2 and c_y in *R. capsulatus* [65]) redox changes monitored at 550–540 nm upon flash excitation of chromatophores derived from the wild type strain (Fig. 5A, WT) reflect this sequence of redox events. In the absence of inhibitors (Fig. 5A, black trace) the fast, unresolved oxidation of cyt *c* is followed by its re-reduction in the ms timescale, via electron donation from the Fe_2S_2 cluster, which in turn receives electrons from QH_2 oxidation at the Q_o site. In agreement with earlier works (e.g. [63]), addition of antimycin had a minimal slowing effect (blue trace) on cyt *c* re-reduction. Since antimycin inhibits all processes at the quinone reduction (Q_i) site, this inhibitor is not expected to affect markedly the re-reduction of cyt *c* after the first flash, which reflects mainly the delivery of the first

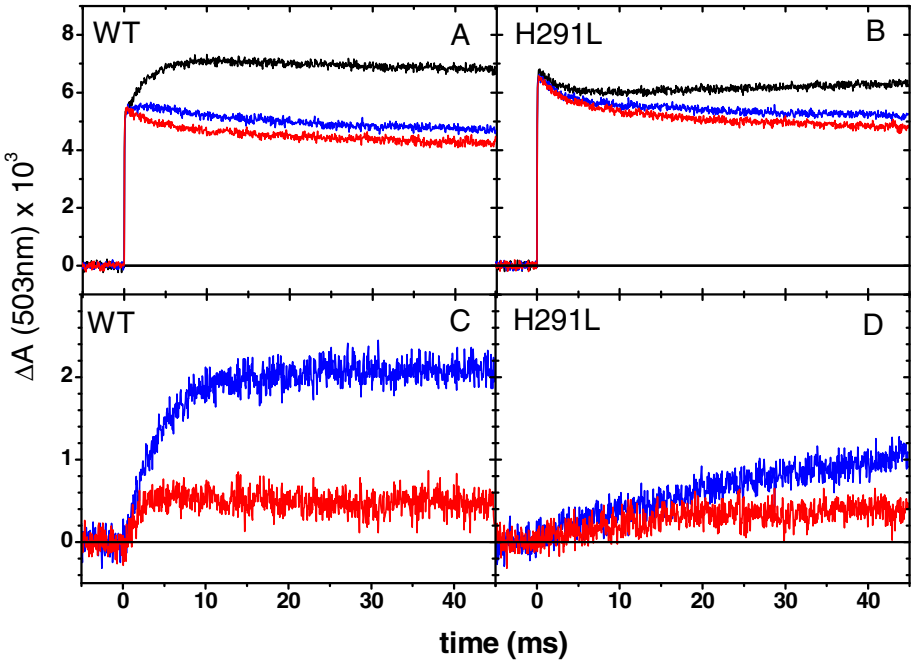

Fig. 4. Kinetics of carotenoid electrochromic signals in wild type and cyt *b* His291Leu mutant strains. The absorption change recorded at 503 nm after a single turnover flash using wild type (WT, panels A and C) and His291Leu (H291L, panels B and D) chromatophores suspended at 40 μM Bchl. The ambient redox potential E_h was poised at 125 mV. The assay conditions were as described in detail under Materials and methods. Panels A and B show the signals obtained in the absence of inhibitors (control, black traces), after addition of 5 μM antimycin (blue traces) and after further addition of 2 μM myxothiazol (red traces), and panels C and D show the phase III components of the carotenoid signals, i.e. the antimycin-sensitive phase (control *minus* antimycin) (blue traces), and the antimycin-insensitive (but myxothiazol-sensitive) phase (antimycin *minus* myxothiazol) (red traces). Traces were the average of 16 (WT) and 32 (H291L) events.

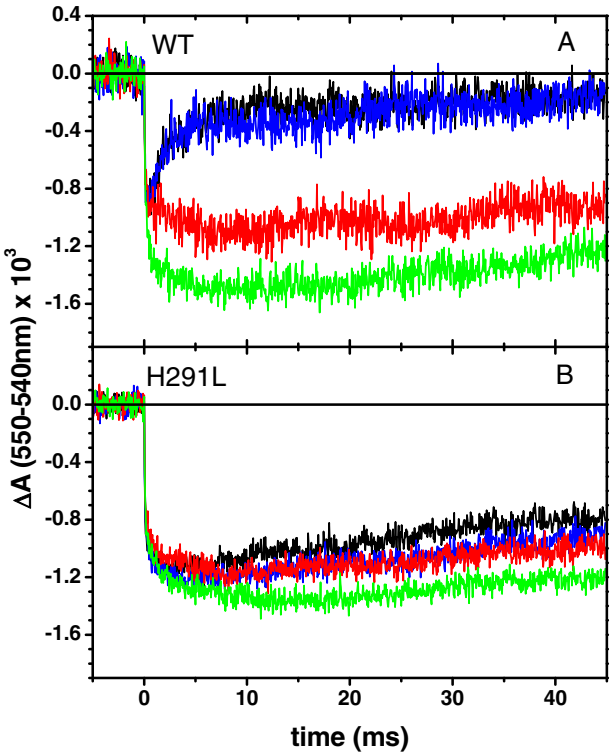

Fig. 5. Flash-induced cyt *c* re-reduction kinetics following a single turnover in wild type and cyt *b* His291Leu mutant strains. Using chromatophore membranes of wild type (WT, panel A) and His291Leu mutant (His291L, panel B) strains, kinetics were recorded at 550–540 nm at an E_h value of 110 mV. Experimental conditions were as in Fig. 4, except that valinomycin was added (at a concentration of 10 μM) to collapse the light-induced membrane potential and avoid any interference with electrochromic effects. Black traces: control in the absence of inhibitors; blue traces: after addition of 5 μM antimycin; red traces: in the presence of 5 μM antimycin and 2 μM myxothiazol; green traces: in the presence of 5 μM antimycin *plus* 1 μM stigmatellin. Traces were the average of 16 (WT) and 32 (H291L) events.

electron from QH_2 oxidation at the Q_o site (see Introduction and [63]). At variance, addition of myxothiazol (red trace) strongly inhibited cyt *c* reduction kinetics, even stimulating the extent of resolved cyt *c* oxidation, by blocking electron donation to the high-potential chain from the Q_o site. A complete inhibition of cyt *c* reduction on the ms timescale, resulting in a further increase of the flash-induced extent of cyt *c* oxidation (green trace), can be observed upon addition of stigmatellin. This Q_o site inhibitor is known to form an H-bonded complex with the reduced ISP Fe_2S_2 cluster to impede its movement towards, and block electron donation to, cyt c_1 [59,64,66].

Quite different cyt *c* reduction kinetics were observed in chromatophores from the H291L mutant (Fig. 5B). In the absence of inhibitors (black trace), cyt *c* reduction kinetics were drastically slowed down, as compared to wild type chromatophores (Fig. 5A), indicating that in the mutant the electron flow through the high potential chain of the complex was strongly impaired. Consistently, while in the wild type chromatophores the addition of myxothiazol (red traces) resulted in a dramatic slowing of cyt *c* re-reduction, and a significant stimulation of its resolved oxidation amplitude, in the mutant (Fig.5B, red trace) myxothiazol had a much smaller slowing effect on the reduction kinetics, as compared to the control (Fig.5B, black trace). Interestingly, at variance with what observed in the wild type, antimycin alone seems to induce a slight retardation of cyt *c* re-reduction in the mutant, accompanied by a slight stimulation of cyt *c* photoxidation (Fig.5B, blue trace). This might be explained by considering that when the semiquinone at the Q_i site is reduced to UQH_2 through the cyt *b* chain, further reducing equivalents are available at the Q_o site in the absence of antimycin, which can contribute to cyt *c* re-reduction. The small effect of antimycin on cyt *c* re-reduction kinetics, due to the suppression of these additional reducing equivalents, is expected to be better resolved in the mutant, where the electron flow along the high potential chain of the cyt bc_1 complex is drastically slowed down already in the absence of inhibitors.

Both in wild type and in the mutant, stigmatellin increased clearly the extent of cyt *c* oxidized after the flash (green trace), as compared to the trace in the presence of myxothiazol, although this effect was smaller in the mutant chromatophores. The fact that such stimulation is clearly observed in chromatophores from the H291L mutant indicated that the ISP extrinsic domain retained a significant mobility in the mutant. However, in view of the slow re-reduction of cyt *c* observed in the mutant even in the absence of inhibitors, as well as in the presence of myxothiazol, we cannot exclude the possibility that this mutation could also slow down the movement of the ISP extrinsic domain, without eliminating it. Therefore, overall data showed that the extremely slow cyt *c* reduction kinetics seen after a single turnover flash in the His291Leu was mainly a consequence of drastically impaired QH_2 oxidation at the Q_o site of cyt bc_1. This agrees with the slowed kinetics of electrogenic events associated with cyt bc_1, as probed by the carotenoid phase III signal (Fig. 4).

Delivery of the second electron derived from QH_2 oxidation at the Q_o site to the low potential chain of cyt bc_1 can be monitored by the heme b_H reduction kinetics induced by a single flash (Fig. 6A and B). The kinetics of this reaction in chromatophores from wild type and His291Leu mutant strains in the presence of antimycin, which blocks electron transfer from reduced cyt b_H to Q (or SQ located at the Q_i site, depending on the first or the second turnover of the Q_o site [67], and on the measuring conditions), were monitored at 560–543 nm (blue traces) at an E_h value of 110 mV (see Materials and methods). Under these conditions, the rate of cyt b_H reduction approaches its maximum, due

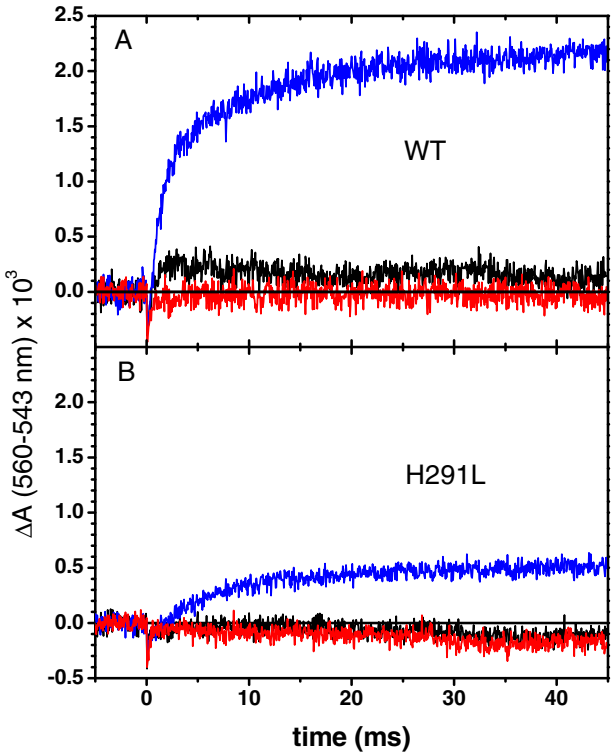

Fig. 6. Kinetics of flash-induced cyt b_H reduction in wild type and cyt *b* His291Leu mutant strains. Using chromatophore membranes of wild type (WT, panel A) and His291Leu (H291L, panel B) strains, kinetics were monitored at 560–543 nm. Experimental conditions and ambient redox poise (E_h) used were as in Fig. 5. Black traces: control in the absence of inhibitors; blue traces: after addition of 5 μM antimycin; red trace: in the presence of 5 μM antimycin and 2 μM mixothyazol. Traces are the average of 16 (WT) or 32 (H291L) events.

to the availability of pre-reduced QH_2 in the quinone pool and pre-oxidation of heme b_H of cyt *b* [68]. Compared to the wild type, both the extent of cyt b_H reduced after the flash, and the initial rate of this reduction were strongly inhibited in His291Leu mutant, with the half time of cyt b_H reduction increasing from ~2 ms in the wild type to ~8 ms in the His291Leu mutant, again closely paralleling carotenoid band shift phase III kinetics.

Similar to above, assuming a differential extinction coefficient ($\varepsilon_{560-543}$) for reduced cyt b_H of 19.5 mM^{-1} cm^{-1}, and taking into account the amount of P of RC photo-oxidized by a single flash, the maximal extent of cyt b_H reduction upon photo-excitation corresponded roughly to 0.51 and 0.14 cyt b_H reduced per photo-oxidized RC in the wild type and the His291Leu mutant strains, respectively. An estimate of the initial rate of cyt *b* reduction yielded values of ~300 and ~60 (cyt b_H reduced) (RC oxidized)$^{-1}$ s^{-1} in wild type and His291Leu chromatophores, respectively. Indeed, addition of myxothiazol completely abolished the reduction of heme b_H in both cases (Fig. 6, red traces). Interestingly, in the absence of inhibitors, a small transient of cyt b_H reduction was detectable only in the wild type (Fig. 6, WT, black traces), in agreement with the slowing of cyt b_H reduction observed in the mutant strain in the presence of antimycin. Indeed, the transient reduction of cyt b_H results from the competition between reduction of the cyt b_H heme via the Q_o site/heme b_L and its re-oxidation by Q (or SQ) at the Q_i site. Thus, in a mutant where delivery of electrons from the Q_o site to the cyt *b* chain is slowed down, the latter reaction is expected to better compete with the former, precluding observation of a transient cyt b_H reduction, which is the case in His291Leu mutant strain.

Taken together, the effects of mutation on the kinetics of cyt *c* re-reduction (Fig. 5), of cyt *b* reduction in the presence of antimycin (Fig. 6), and of phase III of carotenoid shift (Fig. 4) indicate clearly that oxidation of QH_2 at the Q_o site is strongly inhibited in the mutant. The slower kinetic rates observed (unlike the amplitudes of oxidation and reduction) cannot be explained in terms of a diminished expression of the cyt bc_1 in the mutant, or defective assembly of the cyt bc_1 subunits, as these measurements are integral to the complex. In fact, the observation that in the presence of stigmatellin the same extent of cyt *c* oxidation was detected after the flash in wt and in the mutant (Fig. 5) implied that comparable concentrations of total cyts *c* (i.e., cyt c_1 + cyt c_2 + cyt c_y) were photo-oxidized in the examined samples. In spite of this, the re-reduction kinetics of cyt *c* is drastically slowed down in the mutant, demonstrating that the delivery of the first electron from the Q_o site is dramatically inhibited. Consistently, due to the bifurcated nature of the reaction at the Q_o site, a substantial retardation of cyt *b* reduction in the presence of antimycin is seen because the delivery of the first electron is almost blocked in the mutant. In full agreement, a similar effect is also observed for phase III of the carotenoid signal.

The defect in electron transfer events initiated by QH_2 oxidation at the Q_o site of cyt bc_1 in the His291Leu mutant explained why it was unable to support the Ps growth of *R. capsulatus*. Additionally, our results showed that the molecular defect in this mutant was not linked to the mobility of the ISP Fe_2S_2 head domain, or the redox characteristics of the cyt *b* hemes b_L and b_H cofactors, suggesting that it might be more elaborate than the simpler electron transfer events between the cofactors.

Considering that during QH_2 oxidation at the Q_o site of cyt bc_1, the bifurcated cyt *c* re-reduction and cyt *b* reduction involve proton-coupled electron transfer reactions, and that the cyt *b* His291 mutant is a putative Zn ligand [20], a possibility is that during QH_2 oxidation this residue might be critically involved in releasing proton(s) outside of cyt bc_1. In agreement with this notion, in wt chromatophores, Zn^{2+} was found to inhibit cyt *c* re-reduction and phase III of the electrochromic carotenoid signal after a single flash [69], reminiscent of the His291Leu mutant (Fig. 5 and Fig. 4, respectively). Consistently, Zn^{2+} inhibited decylbenzohydroquinone:cyt *c* oxidoreductase activity in purified wt *R. capsulatus* cyt bc_1 [29], again reminiscent of the steady-state activity of His291Leu mutant seen in the absence of Zn (see Supplementary material, Fig. S1).

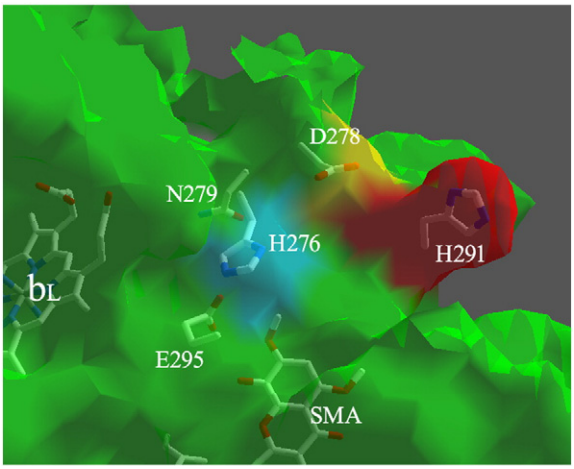

Fig. 7. Surface image of the region of cyt bc_1 where the cyt *b* His291 residue is located. The putative Zn binding residues analyzed for their degrees of conservation (Table 2) are shown by rendering the surface transparent. Among these residues, based on the index of accessibility to the solvent provided by the Swiss-PdbViewer, the His 291 appears to be the most exposed residue (surface colored in red), followed by the considerably less accessible H276 (in blue) and D278 (yellow) residues. SMA and b_L stand for stigmatellin and cyt b_L, respectively. The image was obtained using the Swiss-Pdb Viewer and the PDB file 1ZRT.

Additionally, as depicted in Fig. 7, among the putative Zn^{2+} ligands, His291 is the most solvent-exposed residue, and being in contact with bulk water, might act as the exit residue for proton(s).

3.5. Effects of His291Leu mutation on the flash-induced proton release into the lumen of chromatophores

To further probe the possibility that His291 might be involved in proton(s) egress associated with the oxidation of QH_2 at the Q_o site of cyt bc_1, we studied the kinetics of lumenal acidification after a single turnover flash, as probed by the amphiphilic pH-indicator Neutral red [70]. As detailed in Materials and methods, measurements were performed in the presence of Na-ascorbate and of the redox mediator DAD to establish reducing conditions, comparable to those employed in measurements of the electron transfer kinetics, monitored at E_h values between 110 and 125 mV (Figs. 5 and 6). The terminal oxidase was inhibited by KCN to prevent the oxidation of the redox-buffering system, and oligomycin was added to avoid the rapid escape of protons from the lumen through the ATPase under reducing conditions. The absorbance changes recorded after a flash at 546 nm include, besides the response of Neutral red to pH changes, transient spectral contributions mainly attributable to photo-oxidation and subsequent re-reduction of the RC primary donor P [70]. In order to obtain absorption transients which reflect only the proton release associated with the cyt bc_1 activity, absorption changes after a flash have been recorded in the absence and in the presence of the cyt bc_1 inhibitors myxothiazol and antimycin, and the difference between these signals has been taken to indicate flash-induced pH-transients in the lumen due to QH_2 oxidation at the Q_o site of the cyt bc_1, as previously established with chromatophores from *R. capsulatus* [70] and thylakoids [71]. In Fig. 8 the kinetics of proton release obtained following this procedure were compared over two different time scales in chromatophores from the wt and from the H291L mutant. The absorbance increase observed upon single flash excitation reflects the acidification of the lumen.

The H291L mutation resulted in a strong retardation of the proton release kinetics (Fig. 8A). As shown in Fig. 8B the half-time of lumen acidification, approximately 2.5 ms in the wt chromatophores, increased by almost an order-of-magnitude in the H291L mutant.

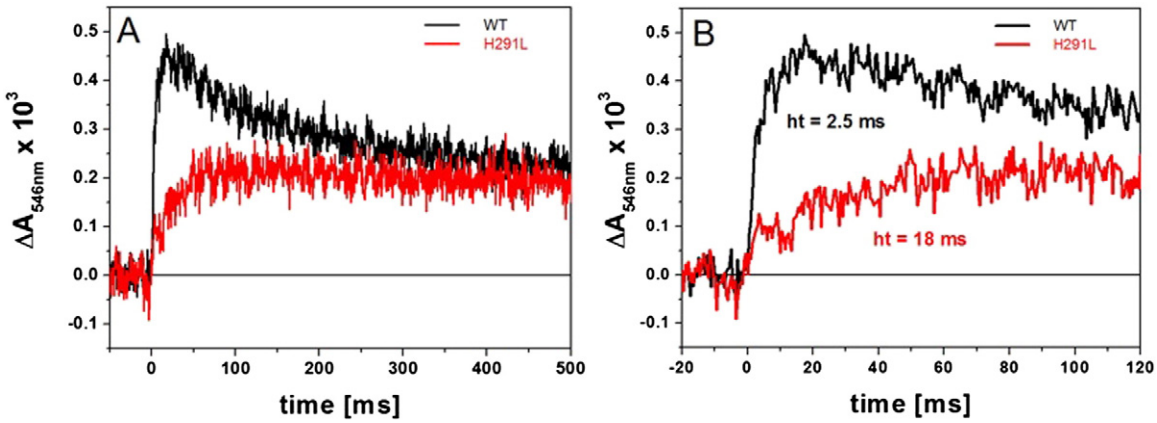

Fig. 8. Kinetics of proton release after a single flash (at $t = 0$) in wt (black traces) and H291L (red traces) chromatophores. Panel B shows the same transients of panel A over an expanded time-scale. Each trace is the difference between flash-induced absorption changes measured at 546 nm in the absence and in the presence of the cyt bc_1 inhibitors antimycin A (5 μM) and myxothiazol (3 μM). Assay conditions are described in Materials and methods.

Such a drastic impairment is fully compatible with the involvement of His291 in proton(s) egress coupled to QH_2 oxidation at the Q_o site of the cyt bc_1.

In view of the proposed role of His291 in proton release from the cyt bc_1, the degree of conservation of this residue in respect to other highly conserved cyt *b* residues [72,25] was assessed by providing as an input the sequence of *R. capsulatus* cyt bc_1 (PDB file 1ZRT, chain C) to the ConSurf server (http://consurf.tau.ac.il/) [73]. From the ConSurf output the degree of conservation of a given residue can be evaluated on the basis of its relative evolutionary rate calculated after Multiple Site Alignment (MSA), which was performed by using the MAFFT-L-INS-i software. Using this method, a negative normalized score with a large absolute value indicates a highly conserved residue. The computed conservation degrees (i.e., normalized scores) of the putative Zn ligands His276, Asp278, Asn279, His291 and Glu295 [20], and of the known to be highly conserved PEWY (Pro294, Glu295, Trp296, Tyr297) loop residues, are shown in Table 2.

Remarkably, the conservation degree of His291 matched closely those of the residues that form the PEWY loop, which are known to be highly conserved in mitochondria, α- and β-Proteobacteria, Aquificae, Chlorobi, Cyanobacteria, and chloroplasts [75], indicating that a His residue in this position is highly favored (Table 2). This observation is in line with the proposal that this residue is involved in proton release to bulk water. If indeed the critical role of His291 is linked to a proton egress pathway from the Q_o site, then the latter path appears to be distinct from an earlier proposed route [76]. This earlier route was based on a high-resolution yeast cyt bc_1 structure, and would involve a propionate on the porphyrin ring of heme b_L, Arg79 of cyt *b* and several fixed water molecules in their vicinity, but not the homologue of *R. capsulatus* H291 residue, which corresponds to Ser at position 268 of yeast cyt *b*.

Table 2
The degree of conservation of selected cyt *b* residues located in the vicinity of His291 expressed as relative evolutionary rate, calculated by using the ConSurf server (http://consurf.tau.ac.il/). Homologous sequences retrieval from the database UniRef90 was performed with a 80% maximal identity cutoff.

Residue	Normalized score[a]	Confidence interval[b]	MSA data[c]
His276	−0.792	−0.889, −0.722	77/77
Asp278	−0.559	−0.772, −0.462	77/77
Asn279	−1.008	−1.032, −0.992	77/77
His291	−1.005	−1.032, −0.992	77/77
Pro294	−0.990	−1.032, −0.976	77/77
Glu295	−1.000	−1.032, −0.992	77/77
Trp296	−0.941	−1.026, −0.914	77/77
Tyr297	−0.982	−1.032, −0.958	77/77

[a] The conservation score is normalized so that the average score for all residues is zero, and the standard deviation is one.
[b] When using the Bayesian method for calculating evolutionary rates, a confidence interval is assigned to each of the inferred evolutionary conservation scores [74].
[c] The number of aligned sequences having an amino acid (non-gapped) from the overall number of sequences at each position.

4. Conclusions

This work described for the first time a detailed characterization of the solvent exposed His291 residue of cyt *b*, which is absolutely required for Q_o site catalysis. Its substitution by a non-protonatable side chain led to drastic loss of Q_o site activity, which was much more pronounced than that earlier observed upon substitution of cyt *b* Glu295 thought to be involved in proton release during QH_2 oxidation, and located in the same region of cyt bc_1 [27–29]. Although the examined His291Leu mutation did not significantly affect the redox potential of cyt b_L and cyt b_H hemes, as determined in chromatophore vesicles, the kinetics of cyt *c* re-reduction, cyt b_H reduction, and proton release to the chromatophore lumen after a single flash were dramatically impaired. The kinetics of cyt *c* re-reduction retained however a significant sensitivity to stigmatellin, suggesting that the drastic impairment of QH_2 oxidation could not be ascribed to the loss of the extrinsic ISP mobility. The electrogenicity of the cyt bc_1 turnover, probed by phase III of the carotenoid phase, was correspondingly inhibited, thus explaining the inability of the mutant to sustain photosynthetic growth. Based on the above summarized observations, on the degree of conservation of His291 as compared to other highly conserved cyt *b* residues in its vicinity, on its large solvent accessibility, and on its putative role in liganding Zn^{2+}, we propose the involvement of this residue in the proton release at the periplasmic surface of cyt bc_1. Undoubtedly, future studies using both membrane-embedded and purified His291Leu variant of cyt bc_1 will address further its critical role in proton egress associated to QH_2 oxidation at the Q_o site.

Supplementary data to this article can be found online at http://dx.doi.org/10.1016/j.bbabio.2016.08.007.

Transparency document

The Transparency document associated with this article can be found, in online version.

Acknowledgments

This work was supported by NIH grant GM 38237 to F.D. Financial support from MIUR of Italy (RFO2014) is gratefully acknowledged by F.F., M.M. and G.V. The authors thank P. Turina (University of Bologna, Italy) for insightful discussions.

References

[1] D. Xia, L. Esser, W.-K. Tang, F. Zhou, Y. Zhou, L. Yu, C.-A. Yu, Structural analysis of cytochrome bc_1 complexes: implications to the mechanism of function, Biochim. Biophys. Acta Bioenerg. 1827 (2013) 1278–1294.
[2] P. Mitchell, Possible molecular mechanism of the protonmotive function of cytochrome systems, J. Theor. Biol. 62 (1976) 327–367.
[3] A.R. Crofts, S. Hong, C. Wilson, R. Burton, D. Victoria, C. Harrison, K. Schulten, The mechanism of ubihydroquinone oxidation at the Q_o-site of the cytochrome bc_1 complex, Biochim. Biophys. Acta Bioenerg. 1827 (2013) 1362–1377.
[4] P.L. Dutton, R.C. Prince, Reaction-center-driven cytochrome interactions in electron and proton translocation and energy coupling, in: R.K. Clayton, W.R. Sistrom (Eds.), The Photosynthetic Bacteria, Plenum Press, New York 1978, pp. 525–570.
[5] A.R. Crofts, Reaction center and UQH_2:cyt c_2 oxidoreductase act as independent enzymes in *Rps. sphaeroides*, J. Bioenerg. Biomembr. 18 (1986) 437–445.
[6] D. Xia, C.-A. Yu, H. Kim, J.-Z. Xia, A.M. Kachurin, L. Zhang, L. Yu, J. Deisenhofer, Crystal structure of the cytochrome bc_1 complex from bovine heart mitochondria, Science 277 (1997) 60–66.
[7] Z. Zhang, L. Huang, V.M. Shulmeister, Y.I. Chi, K.K. Kim, L.W. Hung, A.R. Crofts, E.A. Berry, S.H. Kim, Electron transfer by domain movement in cytochrome bc_1, Nature 392 (1998) 677–684.
[8] G. von Jagow, T.A. Link, Use of specific inhibitors on the mitochondrial bc_1 complex, Methods Enzymol. 126 (1986) 253–271.
[9] A.R. Crofts, The mechanism of the ubiquinol:cytochrome *c* oxidoreductases of mitochondria and of *Rhodopseudomonas sphaeroides*, in: A.N. Martonosi (Ed.), The Enzymes of Biological Membranes, Plenum Publishing, New York 1985, pp. 347–382.
[10] V.P. Skulachev, V.V. Chistyakov, A.A. Jasaitis, E.G. Smirnova, Inhibition of the respiratory chain by zinc ions, Biochem. Biophys. Res. Commun. 26 (1967) 1–6.
[11] T.A. Link, G. von Jagow, Zinc ions inhibit the Q_P center of bovine heart mitochondrial bc_1 complex by blocking a protonatable group, J. Biol. Chem. 270 (1995) 25001–25006.
[12] M.S. Sharpley, J. Hirst, The inhibition of mitochondrial complex I (NADH:ubiquinone oxidoreductase) by Zn^{2+}, J. Biol. Chem. 281 (2006) 34803–34809.
[13] M. Schulte, D. Mattay, S. Kriegel, P. Hellwig, T. Friedrich, Inhibition of *Escherichia coli* respiratory complex I by Zn^{2+}, Biochemistry 53 (2014) 6332–6339.
[14] S.J. Whitehead, K.E. Rossington, A. Hafiz, N.P. Cotton, J.B. Jackson, Zinc ions selectively inhibit steps associated with binding and release of NADP(H) during turnover of proton-translocating transhydrogenase, FEBS Lett. 579 (2005) 2863–2867.
[15] S.J. Whitehead, M. Iwaki, N.P.J. Cotton, P.R. Rich, J.B. Jackson, Inhibition of proton-transfer steps in transhydrogenase by transition metal ions, Biochim. Biophys. Acta 1787 (2009) 1276–1288.
[16] K. Faxen, L. Salomonsson, P. Adelroth, P. Brzezinski, Inhibition of proton pumping by zinc ions during specific reaction steps in cytochrome *c* oxidase, Biochim. Biophys. Acta 1757 (2006) 388–394.
[17] L.M. Utschig, Y. Ohigashi, M.C. Thurnauer, D.M. Tiede, A new metal-binding site in photosynthetic bacterial reaction centers that modulates Q_A to Q_B electron transfer, Biochemistry 37 (1998) 8278–8281.
[18] M.L. Paddock, M.S. Graige, G. Feher, M.Y. Okamura, Identification of the proton pathway in bacterial reaction centers: inhibition of proton transfer by binding of Zn^{2+} or Cd^{2+}, Proc. Natl. Acad. Sci. U. S. A. 96 (1999) 6183–6188.
[19] L. Giachini, F. Francia, A. Mallardi, G. Palazzo, E. Carpenè, F. Boscherini, G. Venturoli, Multiple scattering X-ray absorption studies of Zn^{2+} binding sites in bacterial photosynthetic reaction centers, Biophys. J. 88 (2005) 2038–2046.
[20] L. Giachini, F. Francia, G. Veronesi, D.-W. Lee, F. Daldal, L.-S. Huang, E.A. Berry, T. Cocco, S. Papa, F. Boscherini, G. Venturoli, X-ray absorption studies of Zn^{2+} binding sites in bacterial, avian, and bovine cytochrome bc_1 complexes, Biophys. J. 93 (2007) 2934–2951.
[21] F. Francia, L. Giachini, F. Boscherini, G. Venturoli, G. Capitanio, P.L. Martino, S. Papa, The inhibitory binding site(s) of Zn^{2+} in cytochrome *c* oxidase, FEBS Lett. 581 (2007) 611–616.
[22] G. Veronesi, S.J. Whitehead, F. Francia, L. Giachini, F. Boscherini, G. Venturoli, N.P.J. Cotton, J.B. Jackson, X-ray absorption studies of Zn^{2+}-binding sites in *Escherichia coli* transhydrogenase and its βH91K mutant, Biochim. Biophys. Acta Bioenerg. 1797 (2010) 494–500.
[23] E.A. Berry, Z. Zhang, H.D. Bellamy, L. Huang, Crystallographic location of two Zn^{2+}-binding sites in the avian cytochrome bc_1 complex, Biochim. Biophys. Acta Bioenerg. 1459 (2000) 440–448.
[24] E.A. Berry, L.S. Huang, L.K. Saechao, N.G. Pon, M. Valkova-Valchanova, F. Daldal, X-ray structure of *Rhodobacter capsulatus* cytochrome bc_1: comparison with its mitochondrial and chloroplast counterparts, Photosynth. Res. 81 (2004) 251–275.
[25] M. Degli Esposti, S. De Vries, M. Crimi, A. Ghelli, T. Patarnello, A. Meyer, Mitochondrial cytochrome *b*: evolution and structure of the protein, Biochim. Biophys. Acta 1143 (1993) 243–271.
[26] A.Y. Mulkidjanian, Activated Q-cycle as a common mechanism for cytochrome bc_1 and cytochrome b_6f complexes, Biochim. Biophys. Acta Bioenerg. 1797 (2010) 1858–1868.
[27] A. Osyczka, H. Zhang, C. Mathé, P.R. Rich, C.C. Moser, P.L. Dutton, Role of the PEWY glutamate in hydroquinone-quinone oxidation-reduction catalysis in the Q_o site of cytochrome bc_1, Biochemistry 45 (2006) 10492–10503.
[28] N. Seddiki, B. Meunier, D. Lemesle-Meunier, G. Brasseur, Is cytochrome *b* glutamic acid 272 a quinol binding residue on the bc_1 complex of *Saccharomyces cerevisiae*? Biochemistry 47 (2008) 2357–2368.
[29] D.-W. Lee, Y. El Khoury, F. Francia, B. Zambelli, S. Ciurli, G. Venturoli, P. Hellwig, F. Daldal, Zinc inhibition of bacterial cytochrome bc_1 reveals the role of cytochrome *b* E295 in proton release at the Q_o site, Biochemistry 50 (2011) 4263–4272.
[30] K.A. Gray, E. Davidson, F. Daldal, Mutagenesis of methionine-183 drastically affects the physicochemical properties of cytochrome c_1 of the bc_1 complex of *Rhodobacter capsulatus*, Biochemistry 31 (1992) 11864–11873.
[31] E. Atta-Asafo-Adjei, F. Daldal, Size of the amino acid side chain at position 158 of cytochrome *b* is critical for an active cytochrome bc_1 complex and for photosynthetic growth of *Rhodobacter capsulatus*, Proc. Natl. Acad. Sci. U. S. A. 88 (1991) 492–496.
[32] C. Kulajta, J.O. Thumfart, S. Haid, F. Daldal, H.-G. Koch, Multi-step assembly pathway of cbb_3-type cytochrome *c* oxidase complex, J. Mol. Biol. 355 (2006) 989–1004.
[33] E. Darrouzet, M. Valkova-Valchanova, F. Daldal, The [2Fe-2S] cluster E_m as an indicator of the iron-sulfur subunit position in the ubihydroquinone oxidation site of the cytochrome bc_1 complex, J. Biol. Chem. 277 (2002) 3464–3470.
[34] J. Sambrook, Molecular Cloning: A Laboratory Manual, 3rd ed Cold Spring Harbor Laboratory Press, Plainview, NY, 2001.
[35] B. Khalfaoui-Hassani, P. Lanciano, F. Daldal, A robust genetic system for producing heterodimeric native and mutant cytochrome bc_1, Biochemistry 52 (2013) 7184–7195.
[36] A. Baccarini-Melandri, B.A. Melandri, Partial resolution of phosphorylating system of *Rps. capsulata*, Methods Enzymol. 23 (1971) 556–561.
[37] R.K. Clayton, Spectroscopic analysis of bacteriochlorophylls *in vitro* and *in vivo*, Photochem. Photobiol. 5 (1963) 669–677.
[38] P.K. Smith, R.I. Krohn, G.T. Hermanson, A.K. Mallia, F.H. Gartner, M.D. Provenzano, E.K. Fujimoto, N.M. Goeke, B.J. Olson, D.C. Klenk, Measurement of protein using bicinchoninic acid, Anal. Biochem. 150 (1985) 76–85.
[39] U.K. Laemmli, Cleavage of structural proteins during the assembly of the head of bacteriophage T4, Nature 227 (1970) 680–685.
[40] E. Davidson, T. Ohnishi, M. Tokito, F. Daldal, *Rhodobacter capsulatus* mutants lacking the Rieske FeS protein form a stable cytochrome bc_1 subcomplex with an intact quinone reduction site, Biochemistry 31 (1992) 3351–3358.
[41] D.W. Lee, Y. Ozturk, A. Osyczka, J.W. Cooley, F. Daldal, Cytochrome bc_1-c_y fusion complexes reveal the distance constraints for functional electron transfer between photosynthesis components, J. Biol. Chem. 283 (2008) 13973–13982.
[42] F. Francia, M. Malferrari, S. Sacquin-Mora, G. Venturoli, Charge recombination kinetics and protein dynamics in wild type and carotenoid-less bacterial reaction centers: studies in trehalose glasses, J. Phys. Chem. B 113 (2009) 10389–10398.
[43] F. Francia, M. Dezi, A. Mallardi, G. Palazzo, L. Cordone, G. Venturoli, Protein-matrix coupling/uncoupling in "*Dry*" systems of photosynthetic reaction center embedded in trehalose/sucrose: the origin of trehalose peculiarity, J. Am. Chem. Soc. 130 (2008) 10240–10246.
[44] N.H. Packham, J.A. Greenrod, J.B. Jackson, Generation of membrane potential during photosynthetic electron flow in chromatophores from *Rhodopseudomonas capsulata*, Biochim. Biophys. Acta 592 (1980) 130–142.
[45] D.E. Robertson, E. Davidson, R.C. Prince, W.H. van den Berg, B.L. Marrs, P.L. Dutton, Discrete catalytic sites for quinone in the ubiquinol-cytochrome c_2 oxidoreductase of *Rhodopseudomonas capsulata.* Evidence from a mutant defective in ubiquinol oxidation, J. Biol. Chem. 261 (1986) 584–591.
[46] J.R. Bowyer, S.W. Meinhardt, G.V. Tierney, A.R. Crofts, Resolved difference spectra of redox centers involved in photosynthetic electron flow in *Rhodopseudomonas capsulata* and *Rps. sphaeroides*, Biochim. Biophys. Acta 635 (1981) 167–186.
[47] A. Osyczka, C.C. Moser, F. Daldal, P.L. Dutton, Reversible redox energy coupling in electron transfer chains, Nature 427 (2004) 607–612.
[48] E.H. Evans, A.R. Crofts, *In situ* characterization of photosynthetic electron transport in *Rhodopseudomonas capsulata*, Biochim. Biophys. Acta 357 (1974) 89–102.
[49] N. Guex, M.C. Peitsch, SWISS-MODEL and the Swiss-PdbViewer: an environment for comparative protein modeling, Electrophoresis 18 (1997) 2714–2723.
[50] D. Victoria, R. Burton, A.R. Crofts, Role of the -PEWY-glutamate in catalysis at the Qo-site of the cyt bc_1 complex, Biochim. Biophys. Acta 1827 (2013) 365–386.
[51] P.L. Dutton, Redox potentiometry: determination of midpoint potentials of oxidation-reduction components of biological electron-transfer systems, Methods Enzymol. 54 (1978) 411–435.
[52] A.M. Arutjunjan, Y.A. Kamensky, E. Milgröm, S. Surkov, A.A. Konstantinov, Y.A. Sharonov, Is mitochondrial cytochrome *b*-566/558 a single hemoprotein or two individual components? A magnetic circular dichroism study, FEBS Lett. 95 (1978) 40–44.
[53] K.A. Brown, E.E. Howell, J. Kraut, Long-range structural effects in a second-site revertant of a mutant dihydrofolate reductase, Proc. Natl. Acad. Sci. U. S. A. 90 (1993) 11753–11756.
[54] R. Consonni, L. Santomo, P. Fusi, P. Tortora, L. Zetta, A single-point mutation in the extreme heat- and pressure-resistant Sso7d protein from *Sulfolobus solfataricus* lead to a major rearrangement of the hydrophobic core, Biochemistry 38 (1999) 12709–12717.
[55] N. Sinha, R. Nussinov, Point mutations and sequence variability in proteins: redistributions of preexisting populations, Proc. Natl. Acad. Sci. U. S. A. 98 (2001) 3139–3144.
[56] M.A. Ceruso, A. Grottesi, A. Di Nola, Dynamic effects of mutations within two loops of cytochrome c_{551} from Pseudomonas aeruginosa, Proteins 50 (2003) 222–229.
[57] M.W. Clarkson, S.A. Gilmore, M.H. Edgell, A.L. Lee, Dynamic coupling and allosteric behavior in a nonallosteric protein, Biochemistry 45 (2006) 7693–7699.

[58] P.L. Dutton, J.B. Jackson, Thermodynamic and kinetics characterization of electron-transfer components in situ in *Rps. sphaeroides* and *Rhodospirillum rubrum*, Eur. J. Biochem. 30 (1972) 495–510.
[59] A.R. Crofts, The cytochrome bc_1 complex: function in the context of structure, Annu. Rev. Physiol. 66 (2004) 689–733.
[60] J.B. Jackson, P.L. Dutton, The kinetic and redox potentiometric resolution of the carotenoid shifts in *Rhodopseudomonas spheroides* chromatophores: their relationship to electric field alterations in electron transport and energy coupling, Biochim. Biophys. Acta Bioenerg. 325 (1973) 102–113.
[61] A.R. Crofts, P.M. Wood, Photosynthetic electron-transport chains of plants and bacteria and their role as proton pumps, Curr. Top. Bioenerg. 7 (1978) 175–244.
[62] E.G. Glaser, A.R. Crofts, A new electrogenic step in the ubiquinol:cytochrome c_2 oxidoreductase complex of *Rhodopseudomonas sphaeroides*, Biochim. Biophys. Acta Bioenerg. 766 (1984) 322–333.
[63] A.R. Crofts, C.A. Wraight, The electrochemical domain of photosynthesis, Biochim. Biophys. Acta Bioenerg. 726 (1983) 149–185.
[64] E. Darrouzet, C.C. Moser, P.L. Dutton, F. Daldal, Large scale domain movement in cytochrome bc_1: a new device for electron transfer in proteins, Trends Biochem. Sci. 26 (2001) 445–451.
[65] F.E. Jenney, R.C. Prince, F. Daldal, Roles of the soluble cytochrome c_2 and membrane-associated cytochrome c_y of *Rhodobacter capsulatus* in photosynthetic electron transfer, Biochemistry 33 (1994) 2496–2502.
[66] H. Kim, D. Xia, C.-A. Yu, J.-Z. Xia, A.M. Kachurin, L. Zhang, L. Yu, J. Deisenhofer, Inhibitor binding changes domain mobility in the iron–sulfur protein of the mitochondrial bc_1 complex from bovine heart, Proc. Natl. Acad. Sci. U. S. A. 95 (1998) 8026–8033.
[67] J.W. Cooley, D.W. Lee, F. Daldal, Across membrane communication between the Qo and Qi active sites of cytochrome bc_1, Biochemistry 48 (2009) 1888–1899.
[68] A.R. Crofts, S.W. Meinhardt, K.R. Jones, M. Snozzi, The role of the quinone pool in the cyclic electron-transfer chain of *Rhodopseudomonas sphaeroides*: a modified Q-cycle mechanism, Biochim. Biophys. Acta 723 (1983) 202–218.
[69] S.S. Klishin, W. Junge, A.Y. Mulkidjanian, Flash-induced turnover of the cytochrome bc_1 complex in chromatophores of *Rhodobacter capsulatus*: binding of Zn^{2+} decelerates likewise the oxidation of cytochrome *b*, the reduction of cytochrome c_1 and the voltage generation, Biochim. Biophys. Acta 1553 (2002) 177–182.
[70] A.Y. Mulkidjanian, W. Junge, Calibration and time resolution of luminal pH-transients in chromatophores of *Rhodobacter capsulatus* following a single turnover flash of light: proton release by the cytochrome bc_1-complex is strongly electrogenic, FEBS Lett. 353 (1994) 189–193.
[71] W. Junge, W. Ausländer, A.J. McGeer, T. Runge, The buffering capacity of the internal phase of thylakoids and the magnitude of the pH changes inside under flashing light, Biochim. Biophys. Acta 546 (1979) 121–141.
[72] N. Howell, Evolutionary conservation of protein regions in the protonmotive cytochrome *b* and their possible roles in redox catalysis, J. Mol. Evol. 29 (1989) 157–169.
[73] G. Celniker, G. Nimrod, H. Ashkenazy, F. Glaser, E. Martz, I. Mayrose, T. Pupko, N. Ben-Tal, ConSurf: using evolutionary data to raise testable hypotheses about protein function, Isr. J. Chem. 53 (2013) 199–206.
[74] I. Mayrose, D. Graur, N. Ben-Tal, T. Pupko, Comparison of site-specific rate-inference methods for protein sequences: empirical Bayesian methods are superior, Mol. Biol. Evol. 21 (2004) 1781–1791.
[75] W.-C. Kao, C. Hunte, The molecular evolution of the Q_o motif, Genome Biol. Evol. 6 (2014) 1894–1910.
[76] C. Hunte, H. Palsdottir, B.L. Trumpower, Protonmotive pathways and mechanisms in the cytochrome bc_1 complex, FEBS Lett. 545 (2003) 39–46.